Superfluid properties of the extended Hubbard model with intersite electron pairing

2002 J. Phys.: Condens. Matter 14 9631

(http://iopscience.iop.org/0953-8984/14/41/319)

INSTITUTE OF PHYSICS PUBLISHING JOURNAL OF PHYSICS: CONDENSED MATTER

J. Phys.: Condens. Matter **14** (2002) 9631–9649 PII: S0953-8984(02)36894-2

Superfluid properties of the extended Hubbard model with intersite electron pairing

R Micnas and B Tobijaszewska

Institute of Physics, A Mickiewicz University, Umultowska 85, 61-614 Poznań, Poland

Received 13 May 2002
Published 4 October 2002
Online at stacks.iop.org/JPhysCM/14/9631

Abstract

We study the superfluid properties of short-coherence-length superconductors described by the extended Hubbard model with on-site repulsive and intersite attractive interaction. We have analysed the superfluid stiffness and thermodynamic properties of the model versus electron concentration and pairing interaction on a two-dimensional square lattice with nearest- and next-nearest-neighbour hopping. The effects of phase fluctuations on anisotropic superconductivity of extended s- and $d_{x^2-y^2}$-wave type were examined within the Kosterlitz–Thouless (KT) scenario. The KT critical temperatures were determined and compared with those from the BCS–Hartree–Fock approximation. The Uemura-type plots, i.e. the critical temperature versus zero-temperature phase stiffness, were obtained for both extended s- and d-wave pairings. The states with mixed (s^* and $d_{x^2-y^2}$) symmetry, and in particular the time-reversal breaking state of s + id symmetry, were analysed and the phase diagrams taking into account these states are presented. We also briefly discuss the crossover from BCS to local pair superconductivity for the $d_{x^2-y^2}$-wave pairing. A comparison of the theoretical results with the experimental data, in particular those of T_c versus $\lambda^{-2}(0)$, for high-T_c cuprate superconductors is made.

1. Introduction

Experimental results show that the cuprate high-temperature superconductors (HTSs) are characterized by strong spatial anisotropy. The question of the symmetry of the superconducting order parameter has not been finally solved yet. Several experiments have given contrasting results regarding the s- versus d-wave symmetry in the hole doped cuprate HTS; however the pairing symmetry is characterized by the predominantly $d_{x^2-y^2}$-wave component [1–7]. Moreover, due to a short coherence length and low superfluid density in the underdoped regime, one also expects that the phase fluctuations are important and can have a profound effect on the HTS properties [8–11].

In this paper we study the superconducting properties of systems described by the extended Hubbard Hamiltonian:

$$H = \sum_{i,j,\sigma}(t_{ij} - \mu\delta_{ij})c^{\dagger}_{i\sigma}c_{j\sigma} + U\sum_{i} n_{i\uparrow}n_{i\downarrow} + \tfrac{1}{2}\sum_{i,j,\sigma,\sigma'} W_{ij}n_{i\sigma}n_{j\sigma'}, \tag{1}$$

where t_{ij} is the transfer integral, U is the on-site and W_{ij} is the intersite interaction, μ is the chemical potential and $n_{i\sigma} = c^{\dagger}_{i\sigma}c_{i\sigma}$. The number of electrons per lattice site is given by $n = N^{-1}\sum_{i,\sigma}\langle n_{i\sigma}\rangle$. We will analyse the case of $W < 0$, i.e. the intersite nearest-neighbour (nn) attraction, on a two-dimensional square lattice. This is one of the simplest models of a short-coherence-length superconductor which allows us to consider the case of $d_{x^2-y^2}$ as well as the s-wave symmetry of the gap [12, 13]. It has been widely employed as a phenomenological model in several studies of anisotropic superconductivity in cuprate HTSs [8, 14–32]. The superconductivity and magnetism in the extended Hubbard model (1) with on-site repulsion and intersite attractive interaction have been studied in both the weak-($U < 2zt$) and the strong-($U \gg t$) correlation limits, within various approximation schemes [8, 12–18, 20–22, 26, 27, 30, 31]. The model can be considered as a simple one of oxygen holes pairing in high-T_c cuprates due to a polaronic mechanism [8, 12] or due to purely electronic mechanisms [8, 12] or as an effective model of quasiparticle (antiferromagnetic spin polaron) pairing [19, 23]. An effective near-neighbour attraction has also been used in the study of superconductivity in cuprate HTSs based on the quasiparticle structure derived from the multi-band models [32]. Additionally, within the model (1) inhomogeneous (striped) spin density waves (SDWs) and d-wave superconductivity [30] were obtained and the quasiparticle spectra at the vortex core were studied by using the Bogoliubov–DeGennes equations [31].

The main purpose of this work is to explore further the superconducting properties of the model (1) and analyse the effects of phase fluctuations. As in [12] our study is concerned with a two-dimensional square lattice employing the broken symmetry Hartree–Fock (HF) scheme and considering arbitrary electron density. The phase fluctuation effects are studied within the Kosterlitz–Thouless (KT) scenario. The layout of this paper is as follows. In section 2 we present the formalism and basic equations. The results and detailed discussion of the superfluid density and the critical temperatures are given in section 3.1. The Uemura plots derived within the BCS and KT theory for extended s-(s *-) and $d_{x^2-y^2}$-wave pairings are analysed in section 3.2. This subsection also contains a brief discussion of crossover from BCS to the preformed pair limit in the case of d-wave symmetry. The results for the gap ratio, coherence lengths and the Ginzburg–Landau (GL) ratio are given in section 3.3. The solutions with mixed s + id symmetry, phase diagrams including s *, d and s* + id states and Uemura plots with the symmetry mixing are examined in section 3.4. Conclusions and a comparison with experimental data for cuprate HTSs are given in section 4.

2. Formalism

The self-consistent equations for the superconducting order parameter and the free energy are obtained in the broken symmetry HF–BCS approximation for the Hamiltonian (1) [12], appropriate for the case of weak to intermediate on-site repulsion. For the singlet pairing one obtains the gap equation:

$$\Delta_k = \frac{1}{N}\sum_{q}(-U - W_{k-q})\Delta_q F_q, \tag{2}$$

$$F_q = \frac{1}{2E_q}\tanh\left(\frac{\beta E_q}{2}\right), \tag{3}$$

where W_k is the Fourier transform of W_{ij} and $\beta = 1/k_BT$. The quasiparticle energy is given by $E_q = \sqrt{\bar{\epsilon}_q^2 + |\Delta_q|^2}$, $\bar{\epsilon}_q = \epsilon_q - \bar{\mu}$, with the electron dispersion of $\epsilon_q = -2t(\cos(q_x a) + \cos(q_y a)) - 4t_2 \cos(q_x a)\cos(q_y a)$ for the next-nearest-neighbour (nnn) hopping[1] (t_2), $\bar{\mu} = \mu - n(U/2 + 4W)$. In what follows we consider the nn attraction and the singlet pairing for which the gap function takes the following form for the $d = 2$ square lattice: $\Delta_k = \Delta_0 + \Delta_\gamma \gamma_k + \Delta_\eta \eta_k$, where $\gamma_k = 2(\cos(k_x a) + \cos(k_y a))$ and $\eta_k = 2(\cos(k_x a) - \cos(k_y a))$. The first and second terms refer to the on-site and extended s-wave and the third to the d-wave pairing. The self-consistent equations have the following form [12]:

$$\Delta_0 = -U\Phi_1, \qquad \Delta_\gamma = \frac{|W|}{4}\Phi_\gamma, \tag{4}$$

for the s-wave, and

$$\Delta_\eta = \frac{|W|}{4}\Phi_\eta, \tag{5}$$

for the d-wave symmetry.

In equations (4), (5) Φ_1, Φ_γ, Φ_η, are defined as follows:

$$\Phi_1 = \frac{1}{N}\sum_k \Delta_k F_k, \tag{6}$$

$$\Phi_\gamma = \frac{1}{N}\sum_k \Delta_k \gamma_k F_k, \tag{7}$$

$$\Phi_\eta = \frac{1}{N}\sum_k \Delta_k \eta_k F_k. \tag{8}$$

The above equations have to be solved together with the equation determining the chemical potential μ:

$$n - 1 = -\frac{2}{N}\sum_k \bar{\epsilon}_k F_k. \tag{9}$$

The free energy in the superconducting state is given by

$$\frac{F}{N} = \frac{1}{4}(U - 2|W|\gamma_0)n^2 + \bar{\mu}(n-1) + \frac{1}{N}\sum_k \frac{|\Delta_k|^2}{2E_k}\tanh(\beta E_k/2) - \frac{2}{\beta N}\sum_k \ln(2\cosh(\beta E_k/2)). \tag{10}$$

The density of states (DOS) is given by $N(\omega) = \frac{1}{N}\sum_k (u_k^2 \delta(\omega - E_k) + |v_k|^2 \delta(\omega + E_k))$, $u_k^2 = (1 + \bar{\epsilon}_k/E_k)/2$, $u_k^2 + |v_k|^2 = 1$, and the momentum distribution at $T = 0$ K is $n_k = |v_k|^2$.

The superfluid stiffness ρ_s, which is proportional to $1/\lambda^2$ ($\lambda^{-2} = (16\pi e^2/\hbar^2 c^2)\rho_s$, λ is the London penetration depth), can be obtained from the linear response theory [33, 34] through the relation between the current and the inducing transverse gauge field, and is given by

$$\rho_s^\alpha = \frac{1}{2N}\sum_k \left\{ \left(\frac{\partial \epsilon_k}{\partial k_\alpha}\right)^2 \frac{\partial f(E_k)}{\partial E_k} + \frac{1}{2}\frac{\partial^2 \epsilon_k}{\partial k_\alpha^2}\left[1 - \frac{\bar{\epsilon}_k}{E_k}\tanh\left(\frac{\beta E_k}{2}\right)\right]\right\}, \tag{11}$$

where $f(E_k)$ is the Fermi–Dirac distribution function and $\alpha = x, y$. For the tetragonal system $\rho_s^x = \rho_s^y = \rho_s$. The HF transition temperature is the one at which the gap amplitude vanishes and gives the pair-breaking temperature. When the thermal phase fluctuations of the order

[1] The effect of the Fock term as well as p-wave pairing are not considered here, see [12, 16].

parameter are taken into account, the phase transition generally occurs at a temperature lower than that given by HFA. We assume that in two dimensions this temperature can be determined within the KT scenario [35] and consequently we have estimated it, for each pairing symmetry, from the relation for the universal jump of the superfluid stiffness ρ_s at T_c [35–37][2]:

$$\rho_s(T_c) = \frac{2}{\pi} k_B T_c, \tag{12}$$

where the superfluid stiffness is evaluated from equation (11). Such a method of evaluating T_c has been studied in detail for the two-dimensional attractive Hubbard model, where it provided a valuable estimate for the KT transition temperature [36, 43].

We will also analyse the characteristic lengths in the superconducting state: the GL coherence length ξ_{GL} and the pair correlation length ξ. The GL coherence length (i.e. the spatial extension of the superconducting order parameter) can be obtained through the relation [38]

$$\xi_{GL} = \frac{\Phi_0}{2\pi\sqrt{2}\lambda H_c}, \tag{13}$$

where $\Phi_0 = hc/2e$ is the quantum flux, and the thermodynamic critical field H_c can be calculated from

$$\frac{H_c^2}{8\pi} = \frac{F_n - F_s}{Na^d}, \tag{14}$$

where F_s is given by equation (10) and F_n by $F_s(\Delta_k = 0)$. To determine the pair correlation length one considers the pair correlation function [39]

$$g_{\uparrow\downarrow}(\boldsymbol{r}_1, \boldsymbol{r}_2) = \langle \Psi_\uparrow^\dagger(\boldsymbol{r}_1)\Psi_\downarrow^\dagger(\boldsymbol{r}_2)\Psi_\downarrow(\boldsymbol{r}_2)\Psi_\uparrow(\boldsymbol{r}_1)\rangle - n^2/4. \tag{15}$$

In the BCS state $g_{\uparrow\downarrow}(\boldsymbol{r}_1, \boldsymbol{r}_2) = |\langle \Psi_\uparrow^\dagger(\boldsymbol{r}_1)\Psi_\downarrow^\dagger(\boldsymbol{r}_2)\rangle|^2 = |\mathcal{F}(\boldsymbol{r})|^2$, $\boldsymbol{r} = \boldsymbol{r}_1 - \boldsymbol{r}_2$.

The pair correlation length is given by

$$\xi^2 = \frac{\int g_{\uparrow\downarrow}(\boldsymbol{r})\boldsymbol{r}^2 \,\mathrm{d}\boldsymbol{r}}{\int g_{\uparrow\downarrow}(\boldsymbol{r})\,\mathrm{d}\boldsymbol{r}}. \tag{16}$$

In the ground state, one gets

$$\xi_0^2 = \frac{\frac{1}{N}\sum_k |\nabla\varphi_k|^2}{\frac{1}{N}\sum_k |\varphi_k|^2}, \tag{17}$$

where $\varphi_k = \frac{\Delta_k}{2E_k}$ is the Cooper pair wavefunction. For finite T, φ_k is replaced by $\mathcal{F}_k = \frac{\Delta_k}{2E_k}\tanh(\beta E_k/2)$. ξ is a measure of the pair radius in the condensate and in the $n \to 0$ limit it gives the bound state radius for the two-electron problem. The condensate density is given by $n_0(T) = (1/N)\sum_k \mathcal{F}_k^2$. It should be noted that $n_0(T)$ and $\rho_s(T)$ are different quantities.

By numerical solution of the above equations we have determined the superfluid stiffness and the critical temperatures and constructed the plots of T_c versus $1/\lambda^2(0)$ (the Uemura plots) in the BCS–HFA and KT scenario. We have also evaluated other quantities like the gap ratio, the coherence length, the pair radius and the GL ratio $\kappa = \lambda/\xi_{GL}$ for different pairing symmetries.

3. Results

3.1. Superfluid density and critical temperatures

At first, we analyse the case of nn hopping i.e. $t_2 = 0$. For the d-wave pairing, ρ_s decreases linearly with T, in contrast to the s*-wave pairing, for which the fall in ρ_s is exponential for

[2] This simple way gives us only an upper bound on the actual KT transition (see [36, 37]), since equation (11) does not include the ρ_s renormalization due to topological excitations. A systematic theory should involve a mapping onto an effective X–Y model with renormalized stiffness.

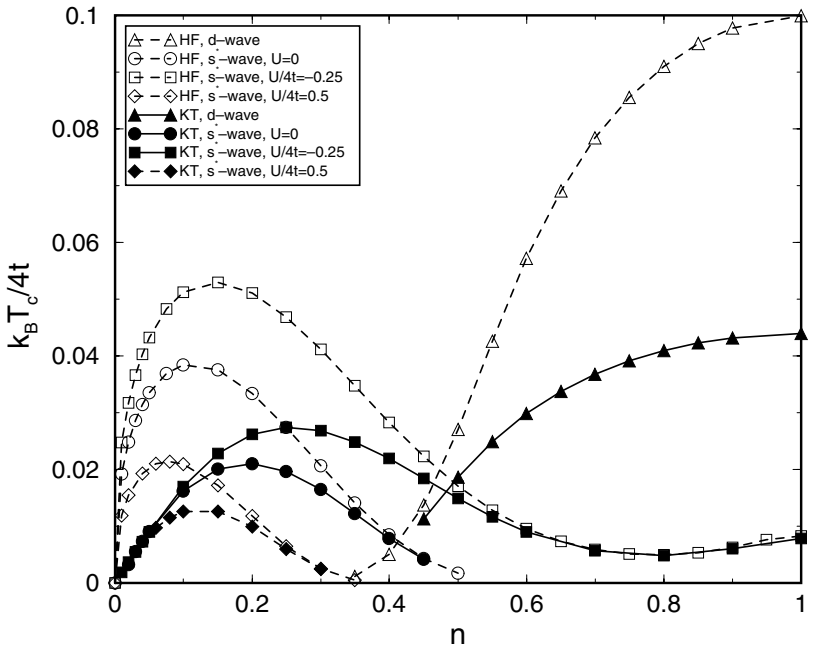

Figure 1. Critical temperatures versus n for nn hopping with nn attraction $|W/4t| = 0.5$ and $U/4t = 0.5, 0, -0.25$, determined within the HFA and KT schemes. Dashed curves denote T_c^{HF} and solid curves are for T_c^{KT}.

low T. The intersection of $\rho_s(T)$ with the straight line $\frac{2}{\pi}T$ yields the KT transition temperature, which is of course smaller than the HF temperature (for which $\rho_s = 0$).

In figure 1 we present the plot of critical temperatures versus n for the nn hopping and $|W|/4t = 0.5$. For small n, the s*-pairing dominates with a characteristic nonmonotonic dependence of $T_c(n)$, while the d-wave pairing dominates near half-filling. The repulsive (attractive) on-site interaction reduces (enhances) T_c for s-wave pairing (figure 1) but has no effect on the d-wave pairing, at least in the BCS–HF approach.

We notice a strong influence of the phase fluctuations on both the s*- and d-wave pairing (for the latter the KT temperatures are even half the HF ones, near $n = 1$, for this value of intersite attraction). Starting from the normal phase, with decreasing temperature, at T_c^{HF} the gap in the energy spectrum opens up and rises with lowering T, but there is no real phase transition to a superconducting state yet. Only at the KT temperature, where the phase coherence sets in, does the transition occur to a phase with bound vortex–antivortex pairs. Between the HF temperature and the KT temperature we have a specific phase in which pairs (of s- or d-waves) are incoherent but the fermionic spectrum has a gap, which can vanish at the nodal points for the pure $d_{x^2-y^2}$ symmetry. This phase could be a finite temperature analogue of the recently discussed 'nodal liquid' phase in quantum disordered d-wave superconductors [40].

We shall now turn to the case of nnn hopping, and the results are displayed in figures 2, 3, 6–9 and 11–13. We have analysed the concentration dependence of $\rho_s(T)$ and T_c for different t_2 values: $t_2 = -0.45t$ (which corresponds to Y123 materials), $t_2 = -0.3t$ (Bi2212 materials) and $t_2 = -0.16t$ (La214 materials). In figure 2 we show the normalized superfluid density (which also yields $\lambda^2(0)/\lambda^2(T)$) versus the normalized temperature T/T_c for the d-wave pairing. We observe a rather weak sensitivity of the normalized penetration depth to the

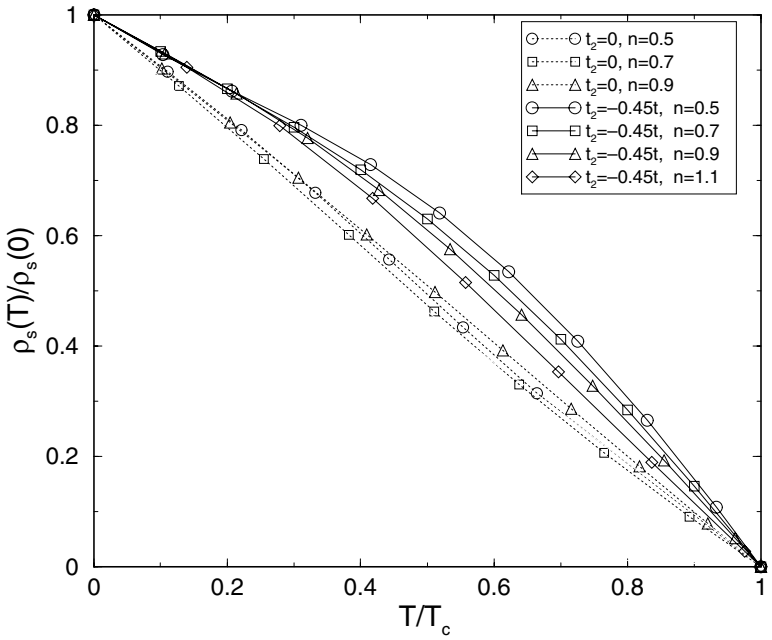

Figure 2. Normalized superfluid density ($\rho_s(T)/\rho_s(0) = \lambda^2(0)/\lambda^2(T)$) versus normalized T/T_c for $d_{x^2-y^2}$ symmetry in HFA and $|W/4t| = 0.5$. The plots are for $t_2 = 0$ and $t_2/t = -0.45$. For the nnn hopping $t_2/t = -0.3$ the curves show similar dependence linear in T/T_c and lie in between.

carrier concentration, especially in the low-temperature regime, which is in agreement with recent experimental studies of the penetration depth in several cuprate HTSs [41][3].

The effect of the nnn hopping on the HF and KT critical temperature appears to be quite important. Figure 3 shows the plots of T_c versus electron concentration n together with concentration dependences of the order parameter and superfluid stiffness at $T = 0$ K. For $t_2 \neq 0$ (e.g. $t_2 = -0.45t$) the d-wave pairing region extends toward lower densities, and the maxima of the critical temperatures are shifted from $n = 1$ more strongly for T_c^{HF} than for T_c^{KT}. For that pairing symmetry, the maximum of T_c^{HF} is controlled by the position of the van Hove singularity in the DOS and for $|t_2| < 0.5t$ the maximum is at $\bar{\mu} \approx 4t_2$, whereas the T_c^{KT} is determined by the superfluid stiffness. For the s *-wave pairing (and $n \leqslant 1$) the maxima of both T_c^{KT} and T_c^{HF} are shifted to higher densities and the T_c^{HF} maximum temperature is higher than for the case of nn hopping. The important point is, as illustrated by the inset in figure 3, that there is a region of densities where $\rho_s(0)$ is smaller than the order parameter, in clear contrast to the conventional weak-coupling superconductors where $\rho_s(0) > \Delta(0)$. This separation of the scales occurs, for sufficiently strong attraction, most easily in the low-density regime for s *-wave pairing. An increase in the nnn hopping amplitude $|t_2|$ implies a similar situation for $d_{x^2-y^2}$ pairing. In general, one observes that if $\rho_s(0) \gg \Delta(0)$, then $T_c \sim \Delta(0)$, whereas in the opposite limit, i.e. if $\rho_s(0) \ll \Delta(0)$, then $T_c \sim \rho_s(0)$.

[3] In particular, it has been obtained from the muon spin rotation (μSR) experiments that the normalized superfluid density is practically doping independent in the range of $0 < T/T_c < 0.35$ and $\lambda^2(0)/\lambda^2(T) \approx 1 - \alpha T/T_c$, with $\alpha = 0.6$ for Y124 and $\alpha = 0.5$ for Y123 materials [41]. Theoretical results from figure 2, for $t_2/t = -0.45$, in the same range of T/T_c yield $\alpha = 0.67$ and $\lambda^2(0)/\lambda^2(T)$ is also independent of concentration n.

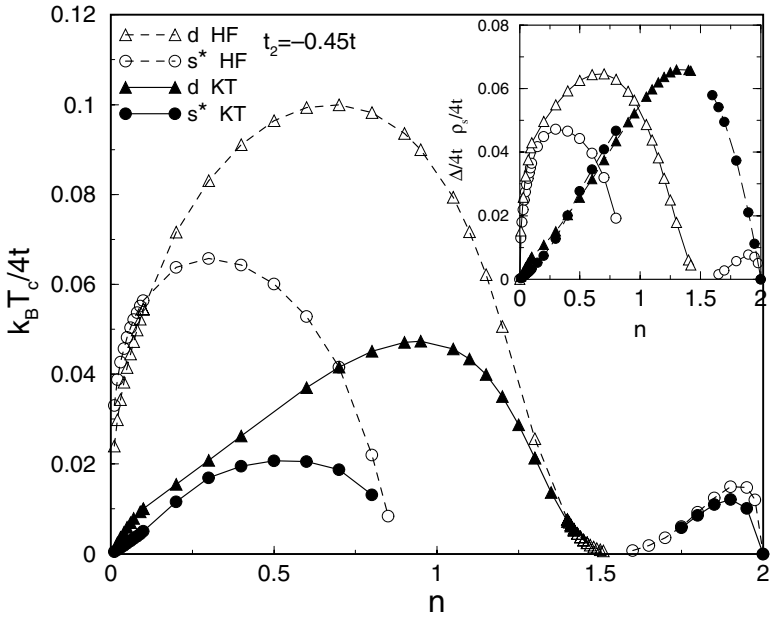

Figure 3. Critical temperatures versus electron concentration for $|W/4t| = 0.5$, $U = 0$ and $t_2/t = -0.45$, in HFA and KT schemes. The inset shows concentration dependences of the order parameter Δ (empty symbols) and superfluid stiffness ρ_s (full symbols) in the ground state.

3.2. Uemura plots

Next, we discuss the Uemura [42]-type plots, i.e. the plots of T_c versus $1/\lambda^2(0)$. We have found that for the nn hopping and with the controlling variable n, only the curves for extended s-wave pairing have a shape similar to the experimental Uemura plots [42] (see figure 4). For the s*-wave pairing and small n, the points determined within KT scenario follow the line $\pi\rho_s(0)/2$, and with increasing density the curves bend below this line, which is an upper bound on the phase ordering temperature. We also see that in the HFA the Uemura scaling $T_c \propto 1/\lambda^2(0)$ is not obeyed.

We notice, however, that the Uemura-type plots can be obtained for the s *- and d-wave symmetry, in the KT scenario, with growing intersite attraction [16] for nn hopping and fixed n, and they are very similar to the crossover plot of T_c versus the coupling strength for the two-dimensional attractive Hubbard model [43].

With the nnn hopping included, we observe that t_2 has a dramatic impact on the behaviour of the plots for d-wave pairing (figure 5). The shape of the plot for d-wave pairing and $t_2 = -0.45t$ is quite different from that for the nn hopping in figure 4. In particular, for larger values of t_2 (close to $t_2 \approx -t/2$) we find a characteristic shape of Uemura plot for d-wave pairing, as we obtained in the case of extended s-wave pairing and nn hopping. We see in figure 5 that for large n, which corresponds to a weak coupling, T_c^{KT} and T_c^{HF} are close to each other, but they become strongly different with lowering density.

We should also point out that when the points collapse on the line $\pi\rho_s(0)/2$, which happens in the dilute limit and for an appropriate strength of the intersite attraction, then the transition to the state with preformed pairs can take place, with the nodeless gap to single-particle excitations for a pure d-wave pairing. This density driven crossover from BCS superconductivity to Bose–Einstein condensation (BEC) of d-wave pairs is very different

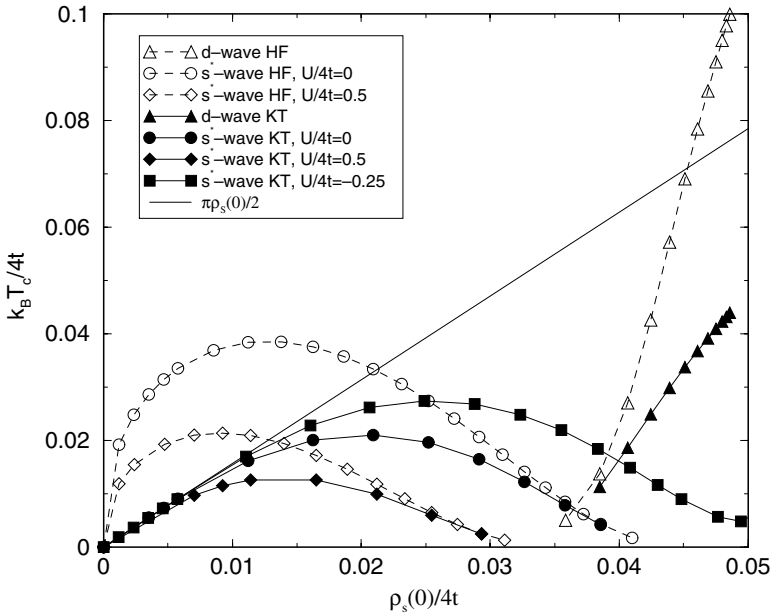

Figure 4. Uemura-type plots (the critical temperature versus superfluid stiffness at $T = 0$) for nn hopping and $|W/4t| = 0.5$. The controlling parameter is electron concentration n. The increasing $\rho_s(0)$ corresponds to an increase in n. Dashed curves with empty symbols denote T_c^{HF}; solid curves with filled symbols are for T_c^{KT}. The curve $\pi\rho_s(0)/2$ is an upper bound on the phase ordering temperature.

from that of s-wave symmetry [16]. Moreover, in the presence of the nnn hopping the local d-wave pairs can have high mobility [45]. In figure 6 we show the behaviour of the DOS in this density driven crossover. In the BCS regime (figure 6(b)) the DOS exhibits a typical d-wave shape with the order parameter amplitude ($\Delta_{max}(0) = 4\Delta_\eta(0)$) determined by the position of the logarithmic singularity. For n in the LP regime (figure 6(a)), the true gap to single-particle excitations opens and is similar to that for s-wave pairing. In such a case, the gap value is given by $2|\bar{\mu} - \epsilon_0|$, and this gap is nodeless in contrast to the order parameter. Beyond the crossover regime, the points in figure 5 deviate from the straight Uemura line and the d-wave order parameter as well as the gap to single-particle excitations has nodes. In figure 5 we also show the plots for s *-wave pairing, which competes with the d-wave state [12, 20, 23]. The increasing on-site repulsion (U) and the nnn repulsion (W_2) will further destabilize this pairing and restrict a possible region of coexistence of s and d solutions[4].

We have also studied the case of $|t_2/t| > 0.5$, for which d-wave pairing takes place even for low density and there is no threshold value of nn attraction to bind the d-wave local pair (LP) in the $n \to 0$ limit. For such values of t_2, the s*-wave pairing can occur for high n only, and for an appropriate strength of nn attraction [12]. In this case, the Uemura scaling for the d-wave symmetry is obeyed in an extended range of concentrations, due to a separation of the scales for the pairing and the phase coherence. As an example, in figure 7 we show the Uemura plots for d-wave pairing and $t_2/t = -1$. For low $\rho_s(0)$ (low n) the plots resemble those for the extended

[4] In the low-density limit the stability of s-wave pairing in two dimensions can be determined from the conditions for the existence of the two-body bound state in an empty lattice [25, 45, 46]. For example, for $U/4t = 1$ and $|W|/4t = 0.5$, s-wave bound state cannot exist if $W_2/4t \geqslant 0.6425$, and the pairing will be suppressed in a dilute limit.

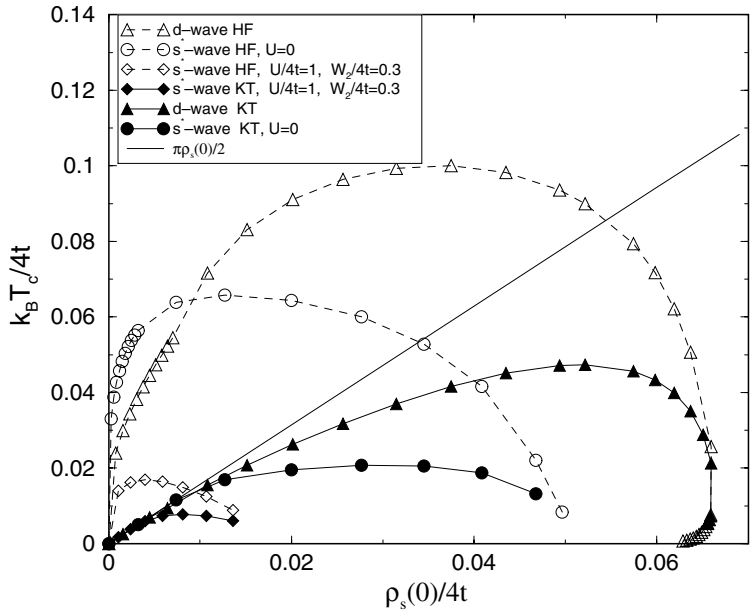

Figure 5. Uemura-type plots for nnn hopping $t_2 = -0.45t$ and $|W/4t| = 0.5$. The controlling parameter is the electron concentration n varying from 0 to 1.5. The dashed curve with empty symbols denotes T_c^{HF}; the solid curve with filled symbols is for T_c^{KT}. The increasing $\rho_s(0)$ corresponds to an increase in n ($n \in [0, 1.45]$). The curve $\pi\rho_s(0)/2$ is an upper bound on the phase ordering temperature. The combined effect of the on-site repulsion ($U/4t = 1$) and the nnn Coulomb repulsion ($W_2/4t = 0.3$) on T_c for s* pairing is shown by open diamonds (HF) and solid diamonds (KT).

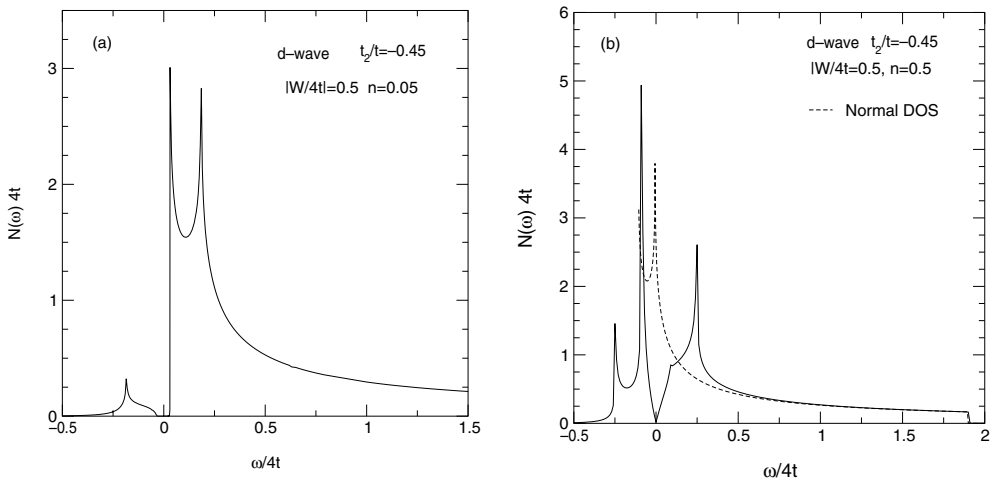

Figure 6. Ground state superconducting DOS versus ω illustrating the density driven crossover from BCS to LP in the case of d-wave pairing for $t_2/t = -0.45$. (a) $n = 0.05$ is for the $d_{x^2-y^2}$ LP case. The superconducting parameters are $\Delta_\eta(0)/4t = 0.0325$, $\bar{\mu}/4t = -0.5802$, $\rho_s(0)/4t = 0.003\,78$. (b) $n = 0.5$ corresponds to the BCS case. The superconducting parameters are $\Delta_\eta(0)/4t = 0.0625$, $\bar{\mu}/4t = -0.4563$, $\rho_s(0)/4t = 0.0256$. The dotted curve shows the DOS in the normal state.

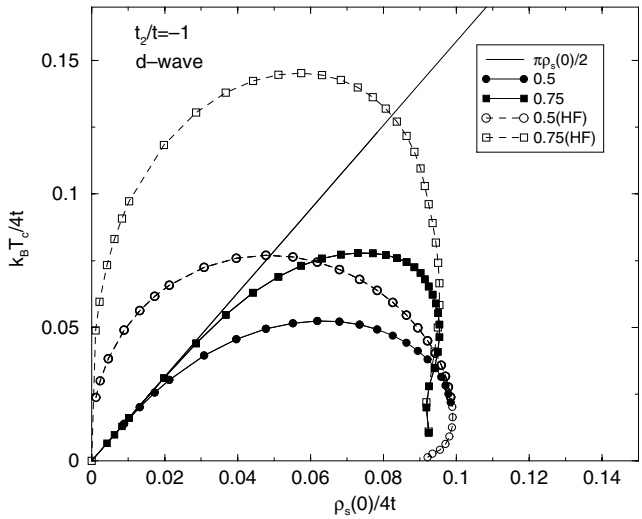

Figure 7. Uemura-type plots for the nnn hopping $t_2/t = -1$, $|W/4t| = 0.5$ and 0.75. The controlling parameter is the electron concentration n ($n \in [0, 1.35]$ for $|W/4t| = 0.5$ and $n \in [0, 1.4]$ for $|W/4t| = 0.75$). Convention as in figure 5.

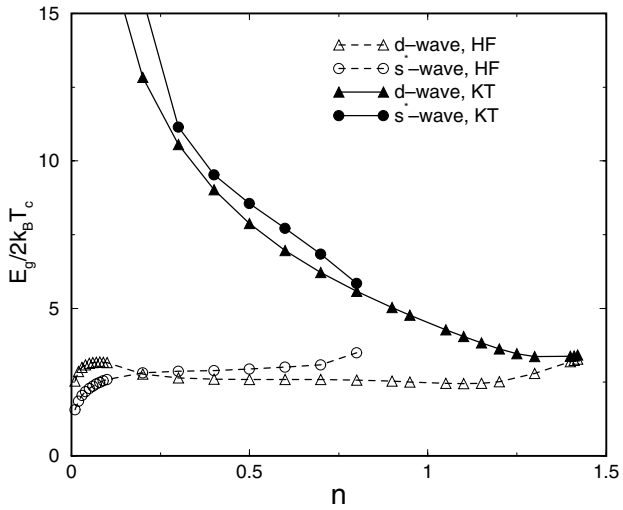

Figure 8. $\Delta_{max}(0)/k_B T_c$ versus concentration n for s* and $d_{x^2-y^2}$-wave pairing symmetries, for $|W|/4t = 0.5$, $U = 0$ and $t_2 = -0.45t$.

s-wave pairing in figure 4. Actually, in both cases the Uemura scaling occurs in the proximity to the band insulator, which in our case is the $n = 0$ point. This further substantiates our finding that for both s *- and d-wave pairing, the Uemura scaling occurs if phase fluctuations are included. An interesting point regarding figure 7 is, that in the low-concentration regime, for any $|t_2/t| > 0.5$, the d-wave gap is nodeless and the analysis of the momentum distribution reveals that the pairing is local and concentrated around the points $(\pm\pi, 0)$, $(0, \pm\pi)$. This is a new, nodeless, d-wave superconducting phase. The nodal points and associated behaviour linear in T of the superfluid density for low T occur for higher n only (see also figure 10). Note that the bottom of the band for $|t_2/t| > 0.5$ is at $\epsilon_{\pi,0} = 4t_2$. Thus, the crossover from the

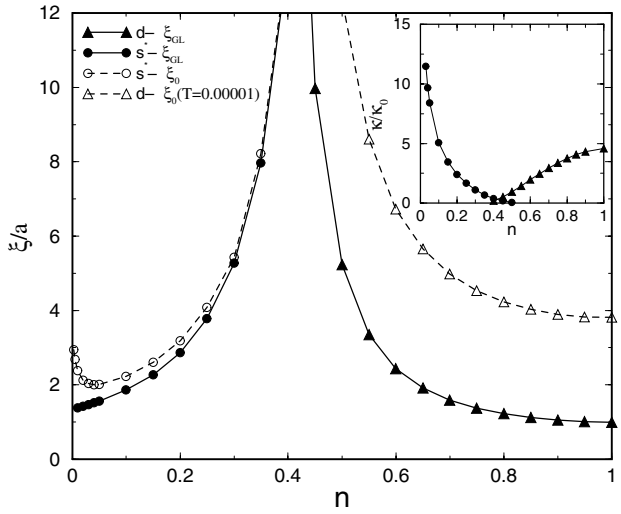

Figure 9. Ginzburg–Landau coherence length (filled symbols) in the superconducting ground state versus concentration n for s*- and $d_{x^2-y^2}$-wave pairing symmetries. $|W|/4t = 0.5$, $U = 0$ and $t_2 = 0$; the pair radius ξ_0 is shown by empty symbols. For d-wave symmetry we evaluated ξ for $k_BT/4t = 10^{-5}$. The inset shows the Ginzburg–Landau ratio versus n ($\kappa_0 = \hbar c/2e\sqrt{\pi a 4t}$).

BCS limit to local d-wave pairs can occur for low n when $\bar{\mu}$ falls below $\epsilon_{\pi,0}$. However, due to the existence of the nodeless BCS-type d-wave state this changeover is different from the case of $|t_2| < 0.5t$, for which we have d-wave pairing with four nodal points, which leads to power law temperature behaviour of the superfluid density and has important consequences for the spectral properties. This BCS–BEC crossover is smooth in contrast to the case of d-wave pairing with nodal points, for which the crossover is continuous but not smooth [15, 16, 44].

The above results concerning the Uemura plots, for both nn and nnn hopping, show a clear separation of the energy scales for intersite pair formation and for the phase coherence in the low-concentration (underdoped) regime (or in the strong coupling)[5], as previously deduced for the s-wave pairing [13, 48, 49] or phenomenologically [13, 42, 47].

3.3. Gap ratio and coherence lengths

The phase fluctuations also modify the mutual stability of s *- and d-wave pairings and yield enhancement of the gap ratio $2\Delta/k_BT_c$ [16]. In figure 8 we show the gap ratios versus concentration n for the case of nnn hopping[6]. It is interesting to observe that the gap ratio for the d-wave pairing (determined by the gap maximum, $E_g = 2\Delta_{max}(0)(\Delta_{max} = 4\Delta_\eta)$) versus n takes a nearly constant value around four to five in the BCS–HF scheme, but in the KT scenario it strongly increases with lowering n and can readily achieve very large values.

The behaviour of the GL coherence length and the pair radius[7] as well as the GL ratio $\kappa = \lambda/\xi_{GL}$ is shown in figure 9. These two lengths, being of the order of a few lattice

[5] This separation of the energy scales for pairing and phase coherence is also supported by the analysis of concentration dependences of the gap and superfluid density at $T = 0$ K [16].

[6] In figure 8 changes in the gap definition when the system passes to the LP limit, which can happen for low n, and/or for sufficiently strong attraction, are not included.

[7] In the case of d-wave symmetry with the nodal quasiparticle spectrum, for evaluation of ξ on the two-dimensional square lattice we have used equation (17) with φ_k replaced by $\mathcal{F}_k = \frac{\Delta_k}{2E_k}\tanh(\frac{E_k}{2k_BT})$, which is a generalization of the pair correlation length to finite temperatures.

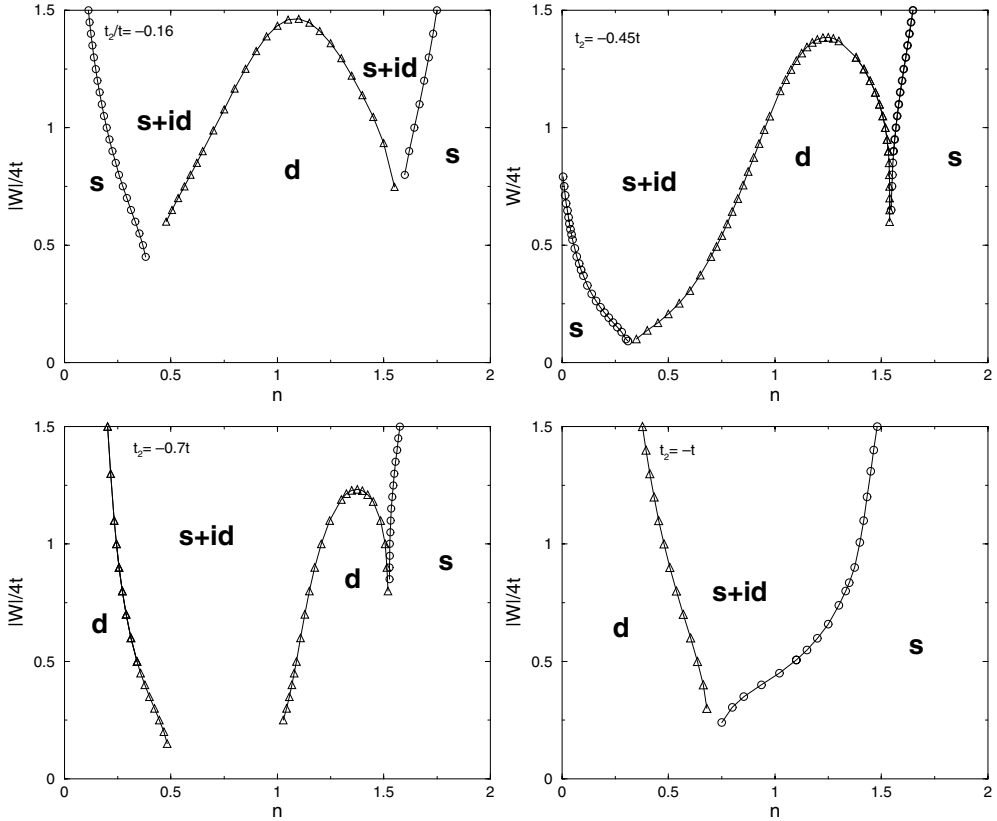

Figure 10. Ground state phase diagrams for $t_2/t = -0.16, -0.45, -0.7$ and -1. $U = 0$. For $|t_2/t| < 0.5$, a pure d-wave state is characterized by four nodal points. For $t_2/t = -0.7$ and -1, a pure d-wave state on the left-hand side will be nodeless, but a pure d-wave state on the right-hand side for $t_2/t = -0.7$ will be characterized by four nodal points. The states s + id and d + is are equivalent.

spacings in the regions where the superconductivity is most stable, increase with decreasing order parameter. For the s *-wave pairing, ξ_{GL} and the pair radius are close to each other; however with $n \to 0$, the pair radius slightly increases (to reach the size of the bound state), thus reflecting the transition to the LP regime (figure 9). In the case of the nnn hopping, ξ_{GL} is nearly constant, in a more extended range of concentrations for the d-wave pairing. The GL ratio shows a strong increase with decreasing concentration, particularly in the region where the separation of scales for pairing and for phase coherence occurs. Such behaviour is characteristic for extreme type II superconductors.

3.4. States with mixed symmetry

The comparably high critical temperatures of s *- and d-wave pairing suggest that there may exist a phase with a mixed symmetry [20, 21]. The general form of the gap in the mixed symmetry state is $\Delta_k = \Delta_k^s + e^{i\alpha}\Delta_k^d$ with a relative phase α (where $\Delta_k^s = \Delta_0 + \gamma_k\Delta_\gamma$ and $\Delta_k^d = \eta_k\Delta_\eta$). It can be shown that the states with $\alpha = 0, \pi$ (s $\pm$ d) or $\alpha = \frac{\pi}{2}, \frac{3\pi}{2}$ (s $\pm$ id) are allowed. In our case, for a tetragonal lattice, the calculations of the free energy indicate that

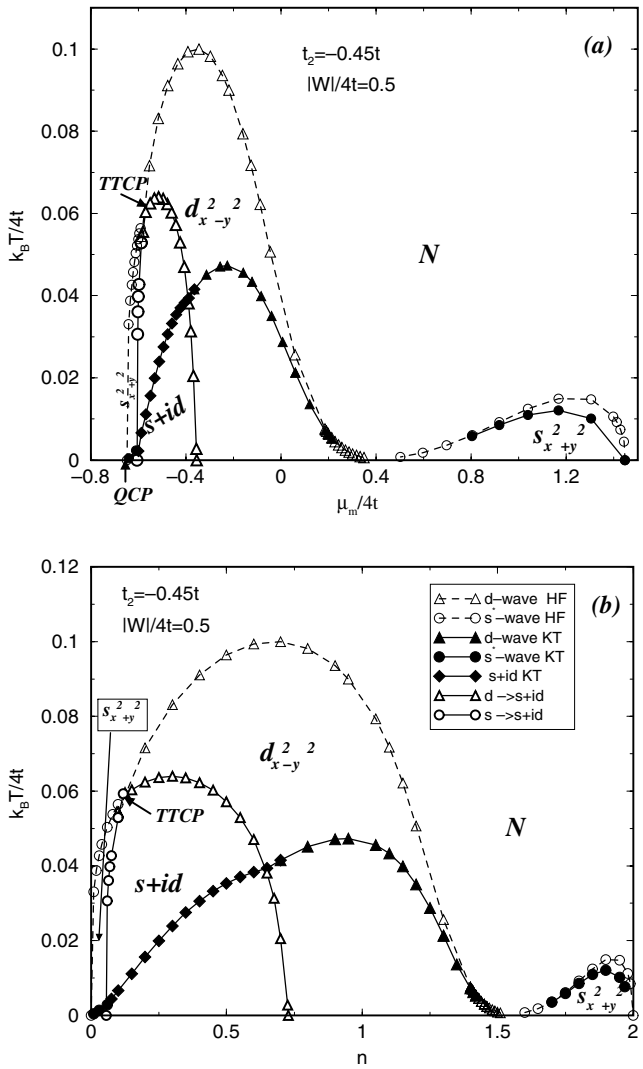

Figure 11. Phase diagrams for the nnn hopping $t_2/t = -0.45$, $|W/4t| = 0.5$, $U = 0$. Panel (a) shows the $(T - \bar{\mu})$ phase diagram ($\mu_m = \bar{\mu}$), while panel (b) the (T–n) phase diagram. Empty symbols denote T_c^{HF}, filled symbols T_c^{KT}. N denotes the normal phase. In the BCS–HFA the four second order lines meet at the tetracritical point (TTCP). The quantum critical point (QCP) at $T = 0$ K can separate the band insulator ($n = 0$) and the s*-wave state.

state s ± id is more stable than s ± d. This conclusion is in accordance with the analysis based on the two-dimensional isotropic Fermi liquid with attraction [50].

In the s + id state, $\Delta_k = \Delta_k^s + \mathrm{i}\Delta_k^d$ and the quasiparticle energy is given by $E_k = \sqrt{\bar{\epsilon}_k^2 + (\Delta_k^s)^2 + (\Delta_k^d)^2}$. The equations for the gap amplitudes $\Delta_0, \Delta_\gamma, \Delta_\eta$, the chemical potential and the free energy are obtained from equations (4)–(10), with the use of the replacement $\Delta_\eta \to \mathrm{i}\Delta_\eta$.

In figure 10 we present the ground state phase diagrams for various values of the nnn hopping: ($t_2/t = -0.16, -0.45, -0.7$ and -1) and $U = 0$. The mixed symmetry states

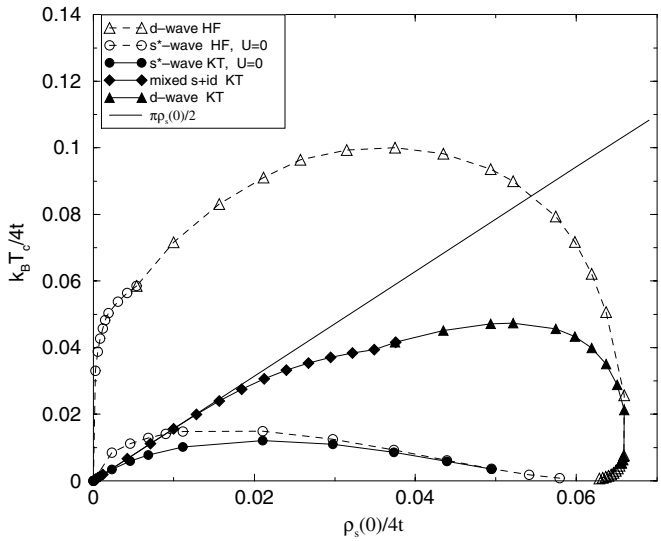

Figure 12. Uemura-type plots for the nnn hopping $t_2 = -0.45t$ and $|W/4t| = 0.5$ with solutions for s + id mixing included. The controlling parameter is the electron concentration n varying from 0 to 2. Convention as in figure 5. Diamonds denote the T_c^{KT} for the state with mixed s + id symmetry; circles starting below the universal line $\pi\rho_s(0)/2$ are for pure s* symmetry for high n ($1.5 < n < 2$) (figure 11(b)).

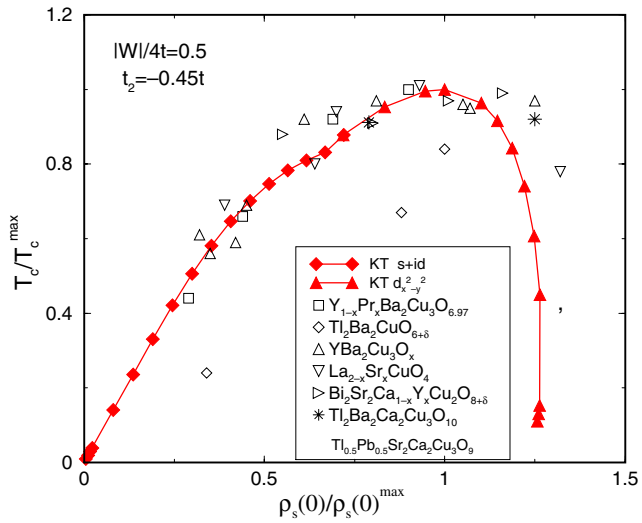

Figure 13. Comparison of experimental results from μSR with theoretical Uemura plots given in figure 12 (see the text).

(This figure is in colour only in the electronic version)

appear when the intersite attraction $|W|$ is sufficiently large and the regions of pure s *- and d-wave states start to overlap. Even if $t_2 = 0$, the state with s + id mixing can be realized for large values of $|W|$. The nnn hopping with $|t_2| < 0.5t$ widens the area of overlaying pure states in the region of small n and narrows it in the region of higher n. The range of pure

s*-wave solutions for small n is strongly restricted by the mixed symmetry state (figure 10). If $|t_2| > 0.5t$, there is a change in the ground state diagrams since the s *-wave pairing is replaced by d-wave pairing for low n, and the d-wave state extends to higher n with growing $|t_2|$. For $|t_2| > 0.5t$, we have the pure $d_{x^2-y^2}$-wave symmetry state in the dilute limit and the mixed s + id (d + is) symmetry is preferred for intermediate concentrations (figure 10). For $t_2 \neq 0$ the phase diagrams lose the $n \to 2-n$ (particle–hole) symmetry; nevertheless, a more general symmetry $t_2/t \to -t_2/t, n \to 2-n$, holds [12].

Figure 11 presents the $(T-\bar{\mu})$ and $(T-n)$ phase diagrams for the case of $t_2 = -0.45t$, ($|W/4t| = 0.5$ and $U = 0$), which show s*, d and s + id phases. In the mixed symmetry state the order parameter has two components: Δ_η and Δ_γ, which, in general, vanish at different temperatures. When the temperature increases the system changes from the mixed s + id symmetry state to the superconducting state with pure symmetry, and finally to the normal state. In the BCS–HFA scheme these transitions are continuous and there are four critical lines which meet at the tetracritical point [51]. We also note an appearance of the quantum critical point on the $(T-\bar{\mu})$ phase diagrams. The position of the QCP is given by the value of the chemical potential $\bar{\mu}/4t = -1 - t_2/t - E_b/8t$, where E_b is the pair binding energy in the two-body problem for an empty lattice. This QCP separates the superconducting phase and the band insulator phase.

In the s + id state, the superfluid stiffness $\rho_s(T)$ is given by equation (11) together with the quasiparticle energy $E_k = \sqrt{\bar{\epsilon}_k^2 + (\Delta_\gamma \gamma_k)^2 + (\Delta_\eta \eta_k)^2}$ and equations for the amplitudes Δ_γ, Δ_η. This $\rho_s(T)$ is subsequently used in equation (12) to determine T_c^{KT}. The calculated values of ρ_s appear to be slightly higher than those for the state with the pure symmetry, therefore the values of T_c^{KT} determined by using equation (12) are a bit higher than those for the pure ordering, in the region of the mixed symmetry. The KT transition temperatures are, however, much lower than those obtained in the BCS–HFA scheme (figure 11). As we mentioned earlier for low n the stability range of pure s* ordering is narrowed by the mixed symmetry state. In figure 11(b), the region of pure s * solution extends from $n = 0$ to 0.1 at $T = 0$. Then for higher n the area of s + id mixing arises. When n still grows the pure d-wave state occurs (for $0.75 < n < 1.45$ at $T = 0$). Finally, for high n the second branch of the pure s* state appears (figure 11).

The above-described changes caused by the symmetry mixing modify the Uemura-type plot as shown in figure 12. In agreement with figure 11, for low n, because of the s + id mixing the T_c^{KT} plot is closer to the universal line $\frac{\pi}{2}\rho_s(0)$. With a further increase of n the pure d-wave state appears and for $n > 1.45$ $\rho_s(0)$ descends and reaches the value 0 for $n = 2$. In this latter concentration range the second branch of the s *-wave solution occurs and this branch is presented in the plot. The left s *-wave branch (for T_c^{KT}) shown in figure 11 is not visible in figure 12 because it is very small. The Uemura plot reported in figure 12 has a characteristic shape of a fly's wing [52]. We note that even with the s–d mixing taken into account, the return of T_c with increasing electron concentration, from 0 to 2, in the Uemura plot is on the s *-wave branch. Let us also add that the mixing will change the Uemura plots for $|t_2/t| > 0.5$ (figure 7). In such a case, however, the state with s + id symmetry will occur for higher n (compare figure 10) and will not influence the universal scaling in a dilute limit. The return will be on the s*-wave symmetry branch.

4. Conclusions

In summary, we have carried out a study of the superconducting properties of two-dimensional extended Hubbard model with intersite attraction for nn and nnn hopping. By invoking the

KT scenario we have systematically analysed the role of phase fluctuations in the anisotropic pairings in two-dimensional short-coherence-length superconductors. We should point out that T_c^{HF} is only a characteristic temperature at which the gap amplitude vanishes and which yields an estimate of the pair formation temperature. The phase transition to the superconducting state can take place at T_c^{KT} at which the phase coherence sets in.

Our results show for the first time that the Uemura-type plots can be obtained for both s*- and d-wave symmetry, in the KT scenario. The reason for the Uemura scaling in systems with low superfluid density such as HTS is a separation of the energy scales for pairing and for phase coherence, in accordance with earlier considerations [47–49]. In this paper we have considered the case of the pure s or d wave as well as the mixed symmetry solutions. Our analysis shows that the states with mixed s + id symmetry with broken time-reversal can be realized in a certain range of density and interactions. The d-wave pairing can be further stabilized by increasing on-site repulsion [12]. Further studies of mixed symmetry solutions are of interest and can be relevant to understanding the nature of the disordered state and crossover to LP behaviour.

We should add that within the BCS–HF and KT theories applied in this paper we can also incorporate the spin fluctuations described by the effective spin exchange of the form $\sum_{ij} J_{ij} \boldsymbol{S}_i \cdot \boldsymbol{S}_j$, $S_i^{\dagger} = c_{i\uparrow}^{\dagger} c_{i\downarrow}$, $S_i^z = \frac{1}{2}(n_{i\uparrow} - n_{i\downarrow})$. J will enter the equations for the extended s- and d-wave pairing as $|W| + \frac{3}{2}J$ [12].

It is of interest to compare our theoretical results for the Uemura plots with the experimental data obtained from the μSR experiments, collected in [42, 52, 53] (see figure 13). For each family of cuprate HTSs we have scaled the experimental T_c (being a function of doping) to T_c^{max} and $\lambda^{-2}(0)$ to the value attained at T_c^{max}. Analogously, we have scaled the theoretical results for T_c and $\rho_s(0)$ given in figure 12. In figure 13 only the KT transition temperatures for the s + id- and d-wave pairing are shown. Given a number of simplifying assumptions, the overall agreement is reasonable, especially in the underdoped regime where the s + id solution is stable; in the optimally doped regime the theory is consistent with the $d_{x^2-y^2}$ pairing. The largest deviations are observed in the overdoped regime.

In the temperature regime $T_c^{KT} < T_c < T_c^{HF}$, the theory predicts a state with phase incoherent pairs, which can correspond to a pseudogap state in underdoped cuprates. One should remark that recent experiments on underdoped Bi2212 and La214, for $T > T_c$, indicate a possibility of transient superconductivity [55] and the existence of single-vortex-type excitations [56], in agreement with the KT scenario.

According to our analysis, the estimated gap ratio $E_g/k_B T_c^{KT}$ for the d-wave pairing can take values close to the experimental ones [54, 57], whereas $E_g/k_B T_c^{HF}$ are much lower (compare figure 8). If we associate the T_c^{HF}, at which the gap closes, with the pseudogap temperature T^*, then the calculated ratio $E_g/k_B T_c^{HF}$, being (nearly constant) of order four to five, is not far from the recently reported ratio $E_g/k_B T^* \approx 4.3$ (BCS d-wave relation), obtained in scanning tunnelling spectroscopy [57].

Let us finally comment on the phase separation which can compete with superconductivity in the case of intersite pairing. The long-range Coulomb interaction or Coulomb interaction extending beyond the nns suppresses the phase separation effects [12]. In this respect, a particular role can be played by the nnn Coulomb repulsion W_2. As mentioned before, this interaction will also reduce the stability of the s-wave pairing (A_1) (by the repulsive s_{xy} component) but has less effect on the $d_{x^2-y^2}$-wave pairing (B_1), since it can only influence the d_{xy} channel transforming according to the B_2 irreducible representation of the C_{4v} point symmetry group. However, $W_2 > 0$ can also lead to stripe charge ordering competing with anisotropic superconductivity [16, 29].

In the present paper, we have used the BCS–HF theory together with the KT scenario to estimate the influence of phase fluctuations in two dimensions on the superconducting T_c. This method of estimating T_c in two dimensions, based on the BCS–HF expression for ρ_s, provides only an upper bound for the actual KT transition [36, 37, 43]. The fluctuations, both quantum and thermal, especially in the case of short coherence length, will renormalize ρ_s and, as a consequence, T_c determined from the KT relation. These important renormalizations, however, are expected to result in relatively small changes in the Uemura-type plots, since the slope is preserved and the bound for the phase ordering temperature is set by $(\pi/2)\rho_s(0)$. Nevertheless, studies going beyond the HF level would be very valuable to assess more completely the fluctuation effects in these short-coherence-length superconductors.

Another problem concerns an improved treatment of electron correlations and an analysis of the competition between anisotropic superconductivity, antiferromagnetism and charge ordered states, which are necessary to fully explore properties of the model analysed in this paper. A more refined analysis of pairing correlations and the state with phase disordered pairs, for short-coherence-length anisotropic superconductors, are also challenging issues of current interest.

Acknowledgments

We would like to thank S Robaszkiewicz and T Kostyrko for useful discussions. This paper is supported by the State Committee for Scientific Research (KBN Poland): project No 2 P03B 154 22.

References

[1] Wu D H *et al* 1993 *Phys. Rev. Lett.* **70** 85
Shen Z-X *et al* 1993 *Phys. Rev. Lett.* **70** 1553
Hardy W N *et al* 1993 *Phys. Rev. Lett.* **70** 3999
[2] Chaudhari P and Lin S-Y 1994 *Phys. Rev. Lett.* **72** 1084
[3] Tsuei C C *et al* 1994 *Phys. Rev. Lett.* **73** 593
[4] Sun A G *et al* 1994 *Phys. Rev. Lett.* **72** 2267
Kleiner R *et al* 1996 *Phys. Rev. Lett.* **76** 2161
[5] Scalapino D J 1995 *Phys. Rep.* **250** 329
[6] Annett J, Goldenfeld J N and Leggett A J 1996 *Physical Properties of High Temperature Superconductors* vol 5, ed D M Ginsberg (Singapore: World Scientific)
[7] Tsuei C C and Kirtley J R 2000 *Rev. Mod. Phys.* **72** 969
[8] Micnas R and Robaszkiewicz S 1997 *High-T_c Superconductivity 1996: Ten Years after the Discovery (NATO ASI Series E vol 343)* ed E Kaldis, E Liarokapis and K A Müller (Amsterdam: Kluwer) p 31 and references therein
[9] Chakraverty B K and Ramakrishnan T V 1997 *Physica* C **282** 290
[10] Emery V J and Kivelson S A 1995 *Phys. Rev. Lett.* **74** 3253
[11] Franz M and Millis A J 1998 *Phys. Rev.* B **58** 14 572
[12] Micnas R, Ranninger J, Robaszkiewicz S and Tabor S 1998 *Phys. Rev.* B **37** 9410
Micnas R, Ranninger J and Robaszkiewicz S 1989 *Phys. Rev.* B **39** 11 653
[13] Micnas R, Ranninger J and Robaszkiewicz S 1990 *Rev. Mod. Phys.* **62** 113
[14] Micnas R, Robaszkiewicz S and Tobijaszewska B 1999 *J. Supercond.* **12** 79 and references therein
[15] Tobijaszewska B and Micnas R 2000 *Acta Phys. Polon.* A **97** 393
Micnas R and Tobijaszewska B 2001 *Proc. 12th School Mod. Phys. on Phase Transitions and Critical Phenomena (Ladek Zdrój, Poland) Acta Phys. Polon.* B **32** 3233
[16] Tobijaszewska B 2001 *PhD Thesis* UAM Poznań
Tobijaszewska B and Micnas R in preparation
[17] Das A N, Konior J, Ray D K and Oleś A M 1991 *Phys. Rev.* B **44** 7680
[18] Spathis P N, Sorensen M P and Lazarides N 1992 *Phys. Rev.* B **45** 7360

[19] Dagotto E *et al* 1994 *Phys. Rev.* B **49** 3548
Nazarenko A *et al* 1996 *Phys. Rev.* B **54** R768
Duffy D *et al* 1997 *Phys. Rev.* B **56** 5597
[20] van der Marel D 1995 *Phys. Rev.* B **52** 1147
[21] O'Donovan C and Carbotte J P 1995 *Phys. Rev.* B **52** 16 208
[22] Eriksson A B, Einarsson T and Östlund S 1995 *Phys. Rev.* B **52** 3662
Maintrup Th, Schneider T and Beck H 1995 *Europhys. Lett.* **31** 231
[23] Feder D L and Kallin C 1997 *Phys. Rev.* B **55** 559
[24] Szabo Z and Gulacsi Z 1997 *Phil. Mag.* B **76** 911
[25] Blaer A S, Ren H C and Tchernyshyov O 1997 *Phys. Rev.* B **55** 6035
[26] Domański T, Wysokiński K I and Ramakumar R 1996 *Phys. Rev.* B **54** 3058
Domański T and Wysokiński K I 1999 *Phys. Rev.* B **59** 173
[27] Martin A M *et al* 1999 *Phys. Rev.* B **60** 7523
[28] Salkola M I and Schrieffer J R 1998 *Phys. Rev.* B **58** 5944
Misawa S 1994 *Phys. Rev.* B **50** 16 623
Misawa S 1996 *Phys. Rev.* B **53** 2241
Demler E, Kohno H and Zhang S-C 1998 *Phys. Rev.* B **58** 5719
[29] Murakami M 2000 *J. Phys. Soc. Japan* **69** 113
[30] Martin I *et al* 2000 *Int. J. Mod. Phys.* B **14** 3567
[31] For example,
Franz M, Kallin C and Berlinsky J 1996 *Phys. Rev.* B **54** 6897
Wang Y and MacDonald A H 1995 *Phys. Rev.* B **52** 3876
Zhu J and Ting C S 2001 *Phys. Rev. Lett.* **87** 147002-I
[32] Gyorffy B L *et al* 1998 *Phys. Rev.* B **58** 1025
Szotek Z, Gyorffy B L and Temmerman W M 2000 *Phys. Rev.* B **62** 3997
[33] Scalapino D J, White S R and Zhang S 1993 *Phys. Rev.* B **47** 7995
[34] Kostyrko T, Micnas R and Chao K A 1994 *Phys. Rev.* B **49** 6158
[35] Kosterlitz J M and Thouless D J 1973 *J. Phys. C: Solid State Phys.* **6** 1181
Kosterlitz J M 1974 *J. Phys. C: Solid State Phys.* **7** 1046
Nelson D R and Kosterlitz J M 1977 *Phys. Rev. Lett.* **39** 1201
[36] Denteneer P J H, An Guozhong and van Leeuwen J M J 1993 *Phys. Rev.* B **47** 6256
van Leeuwen J M J, du Croo de Jongh M S L and Denteneer P J H 1996 *J. Phys. A: Math. Gen.* **29** 41
[37] Chattopadhya B, Gaitonde D M and Taraphder A 1996 *Europhys. Lett.* **34** 705
[38] Fetter A L and Walecka J D 1971 *Quantum Theory of Many-Particle Systems* (New York: McGraw-Hill)
[39] For example,
Pistolesi F and Strinati G C 1996 *Phys. Rev.* B **53** 15 168
Swidzinskij A W 1982 *Prostranstwienno-Nieodnorodnyje Zadaczi Tieorii Swierchprowodimosti* (Moscow: Nauka)
[40] Balents L, Fisher M P A and Nayak C 1998 *Int. J. Mod. Phys.* B **12** 1033
[41] Shengelaya A *et al* 1998 *Phys. Rev.* B **58** 3457 and references therein
[42] Uemura Y J *et al* 1991 *Phys. Rev. Lett.* **66** 2665
Uemura Y J *et al* 1989 *Phys. Rev. Lett.* **62** 2317
Uemura Y J *et al* 1991 *Nature* **352** 605
Uemura Y J 1997 *Physica* C **282–287** 194
[43] Singer J M, Schneider T and Pedersen M H 1998 *Eur. Phys. J.* B **2** 17
Bąk M and Micnas R 1998 *J. Phys.: Condens. Matter* **10** 9029
[44] den Hertog B C 1999 *Phys. Rev.* B **60** 559
Andrenacci N, Perali A, Pieri P and Strinati G C 1999 *Phys. Rev.* B **60** 12 410
[45] Bąk M and Micnas R 1999 *Mol. Phys. Rep.* **24** 168
(Bąk M and Micnas R 1999 *Preprint* cond-matt/9909089)
Bąk M and Micnas R 2000 *Acta Phys. Polon.* A **97** 209
[46] Randeria M, Duan J-M and Shieh L-Y 1990 *Phys. Rev.* B **41** 327
[47] Emery V J and Kivelson S A 1995 *Nature* **374** 434
[48] Doniach S and Inui M 1990 *Phys. Rev.* B **41** 6668
[49] Robaszkiewicz S, Micnas R and Chao K A 1981 *Phys. Rev.* B **23** 1447
[50] Musealian K A, Betrouas J, Chubukov A V and Joynt R 1996 *Phys. Rev.* B **53** 3598
[51] Independently, the tetracritical point has also been obtained within the Ginzburg–Landau analysis in
Wallington J P and Annett J F 2000 *Phys. Rev.* B **61** 1433

[52] Niedermayer C *et al* 1993 *Phys. Rev. Lett.* **71** 1764
Bernhard C *et al* 2001 *Phys. Rev. Lett.* **86** 1614
[53] Czart W, Kostyrko T and Robaszkiewicz S 1996 *Physica* C **272** 51
[54] For example,
Wei J Y T *et al* 1998 *Phys. Rev.* B **57** 3650
[55] Corson J *et al* 1999 *Nature* **398** 2214
[56] Xu Z A *et al* 2000 *Nature* **408** 486
[57] Kugler M *et al* 2001 *Phys. Rev. Lett.* **86** 4911